Relevance of a Tuning-Fork Effect for Temperature Measurements with the Gill Solent HS Ultrasonic Anemometer–Thermometer

HOLGER SIEBERT

Institute for Tropospheric Research, Leipzig, Germany

ANDREAS MUSCHINSKI

Cooperative Institute for Research in Environmental Sciences, University of Colorado, and NOAA Environmental Technology Laboratory, Boulder, Colorado

(Manuscript received 18 July 2000, in final form 8 November 2000)

ABSTRACT

The performance of a new type of sonic anemometer–thermometer (called a *sonic*), the Solent-Research HS, manufactured by Gill Instruments, Lymington, United Kingdom, was investigated. Measurements of the three wind-velocity components u, v, w, and temperature T were taken in the laboratory under quiet conditions and in the field at wind speeds of about 10 m s^{-1}. The power spectra of u, v, w, and T measured in the laboratory follow a $-5/3$ power law at moderate frequencies. At frequencies higher than $\overline{u}/l$ (here $\overline{u}$ is the mean wind speed along a given path of length l), there is a roll-off in all spectra, an expected effect caused by the spatial averaging along the finite pathlength. Over the bandwidth of $f_s/2 = 50$ Hz, the standard deviations due to uncorrelated noise amount to 0.02 m s^{-1} for u, v, and w and to 0.02 K for T. In the field, the spectra of u, v, and w show a clean $-5/3$ power law, except for a flattening at frequencies larger than 30 Hz. The ratio of the spectra of the transverse and longitudinal velocity components was close to 4/3, the ratio predicted by classical theory for isotropic turbulence. The T spectra measured in the field were severely contaminated at frequencies larger than about 5 Hz. Closer inspection of the T time series revealed amplitude-modulated artifacts. These artifacts were presumed to be the result of oscillations of the sonic's pathlengths induced by oscillations of the tower, which was exposed to a turbulently changing wind. The artifacts were reproduced in the laboratory by controlled blows on the sonic's attachment. The mechanical oscillations, which the authors refer to as the *tuning-fork effect,* were measured with a strain gauge attached to the sonic. The tuning-fork effect was observed simultaneously and independently in the strain-gauge measurements and as artifacts in the temperature time series.

1. Introduction

For several decades, ultrasonic anemometers–thermometers (called *sonics*) have been in use for atmospheric turbulence measurements (Kaimal et al. 1968; Mitsuta 1966; Kaimal et al. 1972; Haugen et al. 1975), mainly for research and monitoring of the atmospheric surface layer. A sonic provides the sound velocity and the wind velocity along various, typically three, collocated paths. Typical spatial and temporal resolutions are tens of centimeters and tens of milliseconds. The precision of wind and temperature is on the order of a few centimeters per second and a few tens of millikelvins.

Although the measurement principle is relatively simple, some phenomena must be addressed: flow distortion and blocking effects (Wyngaard and Zhang 1985; Kaimal and Gaynor 1991; Grelle and Lindroth 1994); effects caused by finite pathlengths (Kaimal et al. 1968; Horst 1973) and pulse-averaging effects (Henjes et al. 1999); effects that require crosswind corrections; and the possible presence of cloud or fog droplets (Siebert and Teichmann 2000).

In investigating the quality of velocity and temperature measurements obtained with the sonic Solent-Research HS manufactured by Gill Instruments, Lymington, United Kingdom, two datasets were examined: 1) laboratory measurements under quiet conditions and 2) field measurements in the atmospheric surface layer at moderate wind speed. Spectra and time series of the temperature measured in the field show some artifacts that suggest the relevance of pathlength oscillations at frequencies close to the Nyquist frequency (50 Hz) or higher. In an additional laboratory experiment, ''tuning-fork resonances'' were induced by applying controlled blows to the sonic attachment, to reproduce the artifacts observed in the field. Results are presented and discussed, and some recommendations for future design of sonics are given.

Corresponding author address: Holger Siebert, Institute for Tropospheric Research, Permoserstr. 15, 04318 Leipzig, Germany.
E-mail: siebert@tropos.de

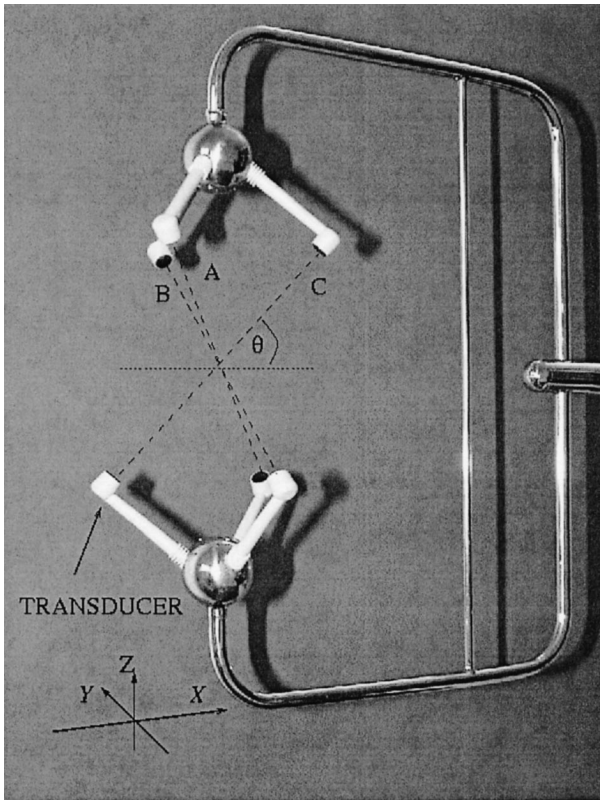

FIG. 1. Sensor head of the Solent HS (Gill Instruments, Ltd. 1998) and axis definition.

2. Data analysis

Three experiments were carried out to investigate the behavior of the Solent HS ultrasonic anemometer–thermometer, from Gill Instruments Ltd., under different conditions. The three measurement axes *A*, *B*, and *C* of this sonic are mounted at an inclination angle $\theta = 48.75°$ and an azimuth angle $\varphi = 120°$ to each other (see Fig. 1). All data were taken at a sampling rate of $f_s = 100$ Hz; that is, the Nyquist frequency is $f_{\mathrm{Ny}} = f_s/2 = 50$ Hz. The distance l between the transducers is 0.15 m for each measurement axis. For further details see the brochure of Gill Instruments Ltd. (1998). The wind data presented in this paper are corrected for flow distortion due to the mounting framework with a matrix calibration described by Gill Instruments Ltd. (1998). A detailed discussion of this standard matrix calibration, other calibration methods, and wind tunnel investigations of flow distortions and transducer shadowing effects for the former Gill Solent (Research II) can be found in Grelle and Lindroth (1994).

In the following, we describe three experiments carried out with the Solent HS. The first experiment was performed under calm wind conditions in a closed laboratory room; the second was performed in the field under moderate wind conditions; the third was performed in the laboratory to reproduce an artifact that was observed in the field.

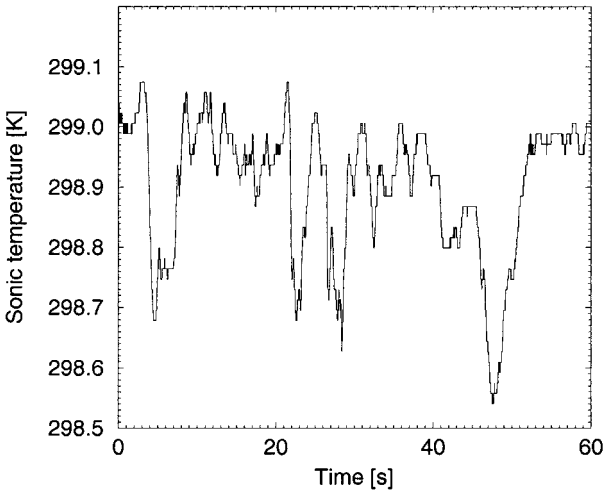

FIG. 2. Time series of sonic temperature *T* measured in the laboratory (run 2).

a. Laboratory measurements under quiet conditions

Time series and spectra of the three velocity components u_A, u_B, and u_C, and of the temperature T were considered. To determine the noise levels, a 60-s dataset of u_A, u_B, u_C, and T was recorded under calm conditions in a closed laboratory room (run 2), and a second dataset was recorded with a protected sensor head (run 4) to reduce the turbulence intensity even further. Data from runs 1 and 3 are not discussed here. All variance spectra of a turbulent quantity q presented in this work are one-sided spectra and related to the corresponding variance σ_q^2 through

$$\sigma_q^2 = \int_0^\infty S_{qq}(f)\, df. \tag{1}$$

1) TEMPERATURE

Figure 2 shows the time series of *T*. During the 60-s observation period (run 2), *T* varied within a range of about 0.6 K. The digitization step of $\Delta_T = 0.01$ K can be clearly seen.

Figure 3 shows the variance spectrum $S_{TT}(f)$ computed from runs 2 and 4. The spectra were computed from a windowed and detrended time series by using a fast Fourier transform algorithm, and applying a von Hann window. The high-frequency part (above 0.1 Hz) of the raw spectrum was smoothed in the frequency domain by averaging over logarithmically equidistant bins.

The noise floor is at $S_{TT}^{(n)} = 1.0 \times 10^{-5}\ \mathrm{K^2\ Hz^{-1}}$. The variance of uncorrelated noise σ_n^2 is the product of the spectral noise floor and the bandwidth (i.e., the Nyquist frequency):

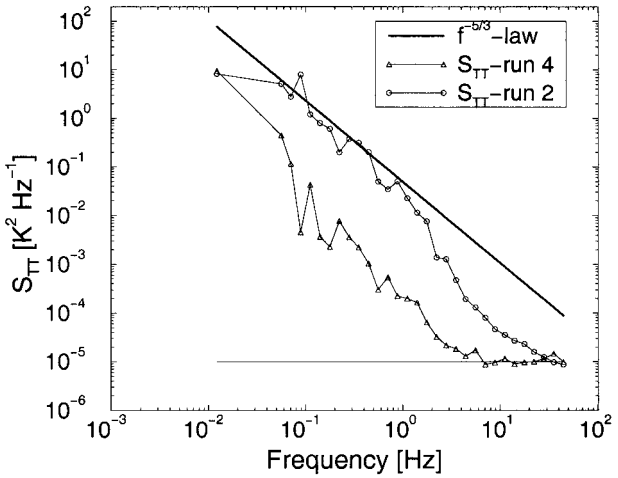

FIG. 3. Power spectra of sonic temperature measured in the laboratory (runs 2 and 4).

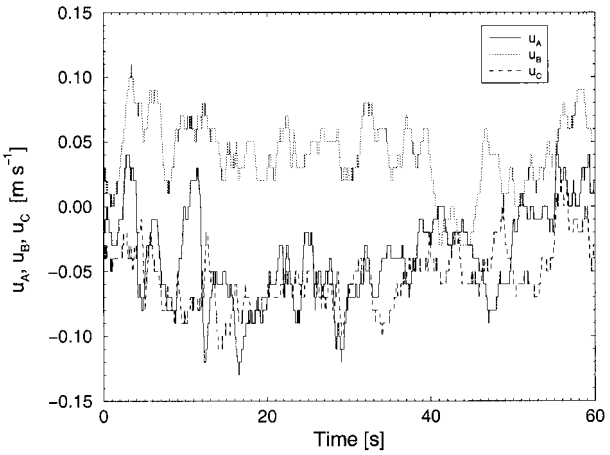

FIG. 4. Time series of the velocity components along the three sonic paths measured in the laboratory (run 2).

$$\sigma_n^2 = S^{(n)} f_{\mathrm{Ny}}. \tag{2}$$

After inserting the value for $S_{TT}^{(n)}$ given above, $\sigma_T^{(n)} = 0.02$ K, the temperature standard deviation due to uncorrelated noise was obtained. Thus, $\sigma_T^{(n)}$ amounts to about two digitization steps.

On the other hand, it is known that the noise floor due to digitization noise S_d is related to the digitization step Δ and the Nyquist frequency f_{Ny} as follows:

$$S^{(d)} = \frac{\Delta^2}{12 f_{\mathrm{Ny}}}, \tag{3}$$

which gives $S_{TT}^{(d)} = 1.7 \times 10^{-7}$ K^2 Hz^{-1} for the sonic thermometer. This value is two orders of magnitude smaller than the system noise floor, which means that digitization does not contaminate the temperature spectra.

2) VELOCITY

Figure 4 shows the time series of u_A, u_B, and u_C, which are the wind vector components measured along the three sonic paths *A*, *B*, and *C*, respectively (run 2). The digitization step Δ_u of the velocity components is 0.01 m s^{-1} for each path, which can be clearly seen. The signals vary between about ± 0.1 m s^{-1} during this 60-s period. Figure 5 shows the variance spectra $S_{uu}(f)$ of the three path velocities of runs 2 and 4. The spectra of both datasets show a noise floor $S^{(n)}$ of about 1×10^{-5} m^2 s^{-2} Hz^{-1} for all three path velocities, which results in a standard deviation due to uncorrelated noise of $\sigma^{(n)} = 2$ cm s^{-1}. That is, $\sigma^{(n)}$ also amounts to about two digitization steps. The noise due to digitization gives $S^{(d)} = 1.7 \times 10^{-7}$ m^2 s^{-2} Hz^{-1}, which is also two orders of magnitude smaller than the system noise floor. The spectra of run 2 drop off for frequencies higher than 1 Hz due to the path-averaging of the sonic. The finite pathlength l becomes relevant when l is no longer small compared with u/f, as is the case, for example, when $u = 0.1$ m s^{-1} and $f = 1$ Hz. A thorough mathematical analysis of the spatial transfer functions associated with the path-averaging effect can be found in Kaimal et al. (1968).

b. Field measurements at moderate wind speed

A field experiment was performed in the atmospheric surface layer to investigate the behavior of the sonic under moderate wind conditions. The experiment took place in Melpitz, the field research station of the Institute for Tropospheric Research, which is about 40 km northeast of Leipzig, Germany. The surrounding area consists of flat grassland without large obstacles for about 1000 m against the prevailing wind direction.

During the measurements, the meteorological conditions were influenced mostly by a high-pressure area over central Europe and a cyclone system over northern Europe. Prevailing winds were about 10 m s^{-1} from the

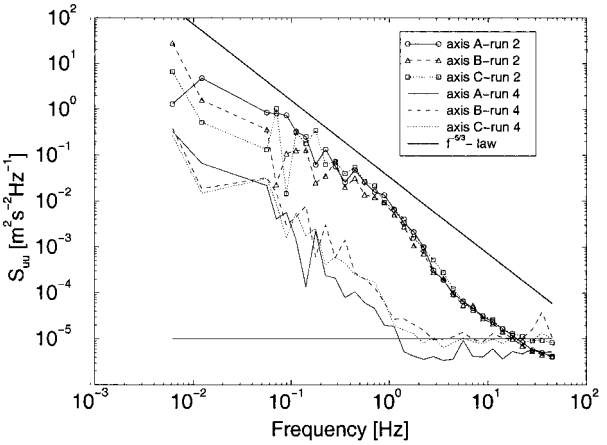

FIG. 5. Power spectra of the three velocity components measured in the laboratory (runs 2 and 4).

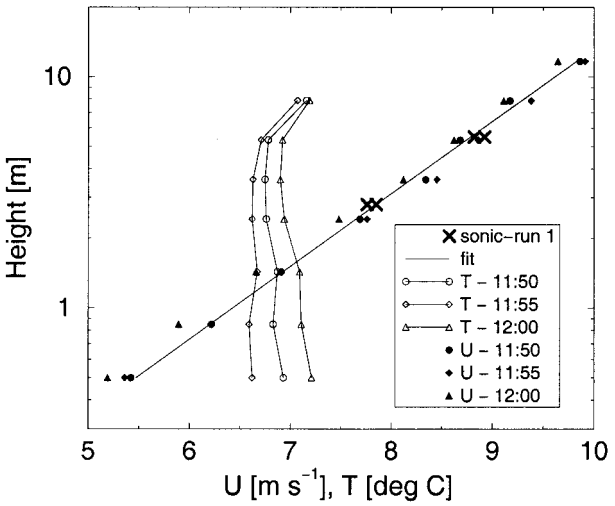

FIG. 6. Vertical profiles of the mean horizontal wind speed $\overline{u}$ and of mean temperature $\overline{T}$ measured in the field under moderate wind conditions. A logarithmic fit is plotted.

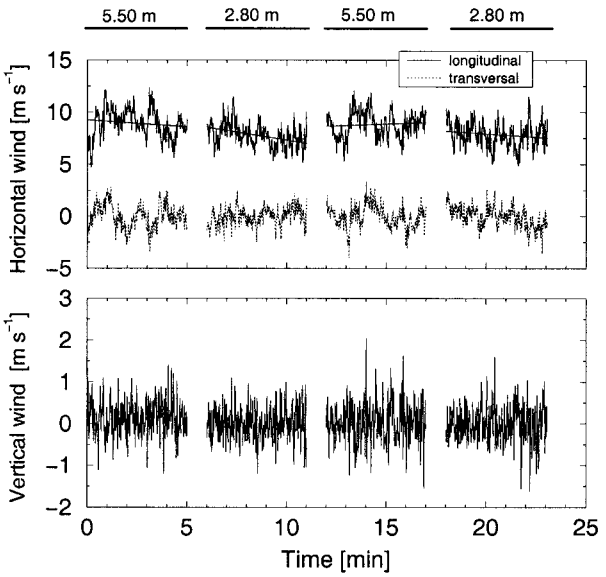

FIG. 7. Time series of the horizontal streamwise and transverse wind velocity components u and v, and of the vertical wind velocity component w, measured in the field at two different heights. The time series data were smoothed by a running mean over 100 points; for the longitudinal components a linear trend is plotted.

southwest in the experimental area. The sky was covered with stratocumulus clouds; there was no rain. In addition to the sonic data, the temperature T and horizontal wind velocity u were measured with a platinum-wire thermometer (Pt-100) and a cup anemometer mounted on a 12-m tower. The additional data are available as 5-min mean values in eight logarithmic heights. Figure 6 shows the vertical profiles of mean wind and temperature at the beginning of the experiment (run 1). The temperature was nearly independent of height, while the wind followed a logarithmic profile for neutral stratification:

$$\overline{u}(z) = \frac{u_*}{\kappa} \ln\left(\frac{z}{z_0}\right). \tag{4}$$

Fitting the mean wind speed data to Eq. (4) provided a roughness length $z_0 = 1.5$ cm and a friction velocity $u_* = 0.6$ m s^{-1}, where we have assumed a von Kármán constant $\kappa = 0.4$. The sonic was mounted at a mast in two interchangeable heights [2.80 and 5.50 m above ground level (AGL)]. The X direction of the sonic (see Fig. 1) was oriented in the mean wind direction within about 45° to minimize flow distortions due to the mast and other mounting framework. Each run consisted of four 5-min periods; after every period the height of the sonic was changed. Two measurements at each height were performed. The wind vector components referred to in the following subsections are defined as u for the streamwise wind-vector component, v for the lateral component, and w for the vertical component. A coordinate transformation is performed in two steps. First u is rotated into the mean wind direction, that means $\overline{v} = 0$. The second rotation sets $\overline{w} = 0$. This and other types of coordinate transformations are described and discussed in more detail in Wilczak et al. (2000).

1) VELOCITY SPECTRA

Figure 7 shows the time series of u, v, and w. The data were sampled at $f_s = 100$ Hz. The time series data were smoothed with a running mean over 100 points to reduce scatter. The 1-min gaps in the time series are due to manual changes of the sonic's altitude.

The velocity varies between 5 and 12 m s^{-1} for the longitudinal component and between −1.6 and +1.6 m s^{-1} for the vertical. The mean wind $\overline{u}$ (longitudinal) and the standard deviation σ_u are given in Table 1 for each sample. For both periods, the mean wind at 5.50 m is about 1 m s^{-1} higher than that at 2.80 m, which fits well with the logarithmic wind profile observed from the low-frequency measurements (see Fig. 6). Since

$$u_* = \frac{\overline{u}(z_1) - \overline{u}(z_2)}{\ln\left(\frac{z_1}{z_2}\right)}\kappa, \tag{5}$$

the friction velocities derived from the two height pairs of run 1 are about 0.4 and 0.5 m s^{-1}. These values agree well with the friction velocities derived from the sonic data (see Table 1) by the covariance method through

TABLE 1. Mean values and standard deviations of temperature T, wind velocity u, and friction velocity u_* measured in the field at two heights under moderate wind conditions.

Height (m)	$\overline{u}$ (m s^{1})	σ_u (m s^{-1})	u_* (m s^{-1})	T (°C)	σ_T (K)
5.50	8.92	1.39	0.45	5.52	0.09
2.80	7.76	1.10	0.47	5.54	0.12
5.50	8.82	1.21	0.39	5.78	0.10
2.80	7.85	1.17	0.53	5.71	0.09

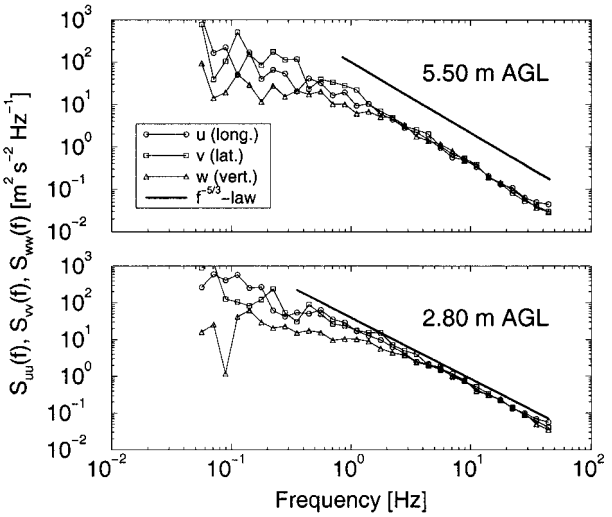

FIG. 8. Power spectra of the three wind velocity components u, v, and w, at (bottom) 2.80 m and (top) 5.50 m AGL derived from field measurements (run 1). The spectral estimates are averages of the raw spectral estimates over logarithmically equidistant bins with a width of one-tenth of a decade.

$$u_*^2 = \sqrt{\overline{uw}^2 + \overline{vw}^2}. \tag{6}$$

Figure 8 presents the power spectra of the three wind components at the two different heights. All spectra show an inertial subrange. While the vertical and lateral components follow the $f^{-5/3}$ law nicely up to the Nyquist frequency, the longitudinal component flatten close to the Nyquist frequency. This effect is possibly caused by the transverse oscillations of the vertical boom, which induces artificial wind speeds in the longitudinal direction.

Figure 8 shows that at low frequencies, the spectra do not decrease as steeply as at higher frequencies. The flattening of the surface-layer spectra at frequencies comparable to $f_0(z) = \overline{u}(z)/z$ is a well-known phenomenon (e.g., Kaimal et al. 1972). Muschinski and Roth (1993) defined an effective cutoff frequency $f_c(z)$ such that, by definition, the integral over the inertial-range asympote over all frequencies larger than $f_c(z)$ equals the variance of the respective fluctuating quantity at the altitude z. Muschinski and Roth (1993) find

$$f_c(z) = \frac{\overline{u}(z)}{4z}. \tag{7}$$

At $z = 2.80$ m, where we have $\overline{u} = 7.8$ m s^{-1}, we obtain $f_c = 0.7$ Hz; and at $z = 5.50$ m, where we have $\overline{u} = 8.9$ m s^{-1}, we find $f_c = 0.4$ Hz. These two estimates of f_c agree reasonably well with the frequencies at which the transition from the energy-containing range to the inertial range occurs in Fig. 8. That is, the deviations of the observed spectra from inertial-range behavior at frequencies comparable to and lower than f_c can be attributed to the finite measurement altitudes.

The large scatter at both heights for frequencies below 0.1 Hz is due to the poor statistics of a 5-min run. The relative behavior of the longitudinal (u) and transversal (v, w) spectral components in the inertial subrange is discussed in section 2b(3).

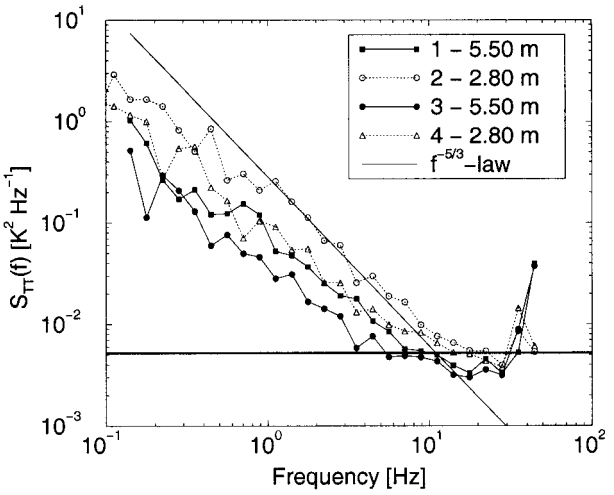

FIG. 9. Temperature power spectra derived from field measurements at two different heights (run 1).

2) TEMPERATURE SPECTRA

Figure 9 shows the temperature power spectra $S_{TT}(f)$ obtained from runs 1 and 4. The spectra show an inertial subrange with a slope of $-5/3$ up to about 5–10 Hz. At higher frequencies, the spectra begin to flatten, and they show a significant peak around the Nyquist frequency. The plateau of $S_{TT}(f) \approx 5 \times 10^{-3}$ K^2 Hz^{-1}, if interpreted as white noise, leads to a standard derivation of about 0.5 K, which is much higher than that obtained in the laboratory under calm wind conditions. To investigate this behavior in more detail, spectra were plotted with a linear frequency and averaged only by a running mean over 10 samples to reduce scatter (see Fig. 10). All datasets show a significant peak between 46 and 47 Hz. A second peak can be seen around 33 Hz for the data sampled at a height of 5.50 m; the data taken at 2.80 m show a peak near 31 Hz. The first datasets (runs 1–4) also show a third peak around 20 Hz independent of the installation height. Figure 11 shows a sequence of the temperature time series during run 1 at 5.50 m. Also shown are u and v and the roll and pitch angles α_X and α_Y. The short periods of very high temperature fluctuations correlate well with rapid changes in the wind components. Therefore, portions of the temperature time series are enlarged to show these events in more detail. Detail A shows a 7-s sequence. On the right is 1 s of the time series with a beat of about 7–8 Hz, which is enlarged again in detail C. The high-frequency oscillation around the Nyquist frequency can also be seen on the left, which is enlarged again in detail B.

Figure 12 shows the power spectra of α_X and α_Y. These data are sampled only with 10 Hz. Therefore, the peaks of the temperature spectra observed in Fig. 10 cannot be seen directly in the inclinometer data. How-

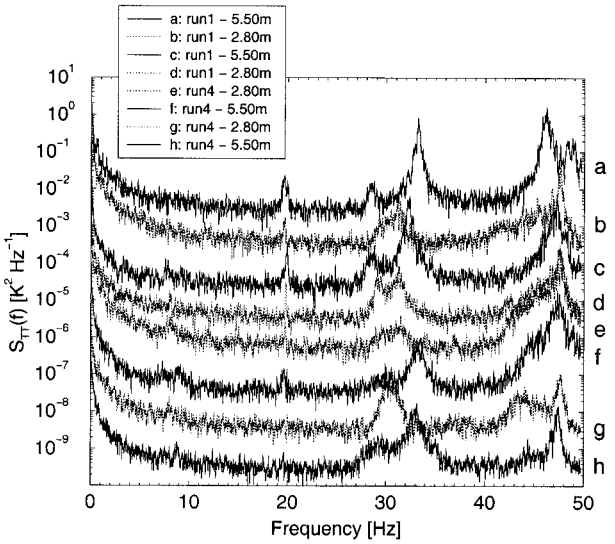

FIG. 10. Temperature power spectra from eight datasets derived from field measurements at two different heights (runs 1 and 4). All spectra are shifted one order of magnitude from the one above; the top one has the original amplitude.

ever, the beat frequency of 7–8 Hz seems to be folded back at the Nyquist frequency and can be seen in the spectra around 2–3 Hz.

3) LOCAL ISOTROPY

For the inertial subrange of locally isotropic and homogeneous turbulence, classical turbulence theory predicts a 4/3 ratio between the spectra of lateral and longitudinal velocity components, that is

$$\frac{S_{vv}}{S_{uu}} = \frac{S_{ww}}{S_{uu}} = \frac{4}{3}. \tag{8}$$

Kaimal et al. (1972) discussed local isotropy in the atmospheric surface layer for a wide range of stability parameters. For a better comparison with these data, our calculated ratios in Fig. 13 are presented as a function of the normalized frequency $n = fz/U$, with the measurement height z and the mean wind U. Figure 13 (bottom) shows that the ratio S_{ww}/S_{uu} comes close to 4/3 in a range between the dimensionless frequency of $n = 2$ to 10. At lower and higher frequencies, values smaller than 4/3 are obtained. At lower frequencies, the deviation is caused by the suppression of w fluctuations at length scales comparable to and larger than the measurement height. For S_{vv}/S_{uu} (Fig. 13, top) large scatter occurs below $n = 1$, but for n larger than 1, its behavior is similar to that of S_{ww}/S_{uu} (Fig. 13, bottom). At higher frequencies, the spectral transfer function that describes the effect of low-pass filtering when the resolved wavenumbers k come close to the inverse of the soundpath length l drops off more rapidly with frequency for w than the transfer function for u. Kaimal et al. (1968) calculated spectral transfer functions for all three velocity components, which become significantly different from one another for $kl \geq 2$, which corresponds to the dimensionless frequency of $n = 12$ in Fig. 13. The transfer functions of the sonic examined in this paper,

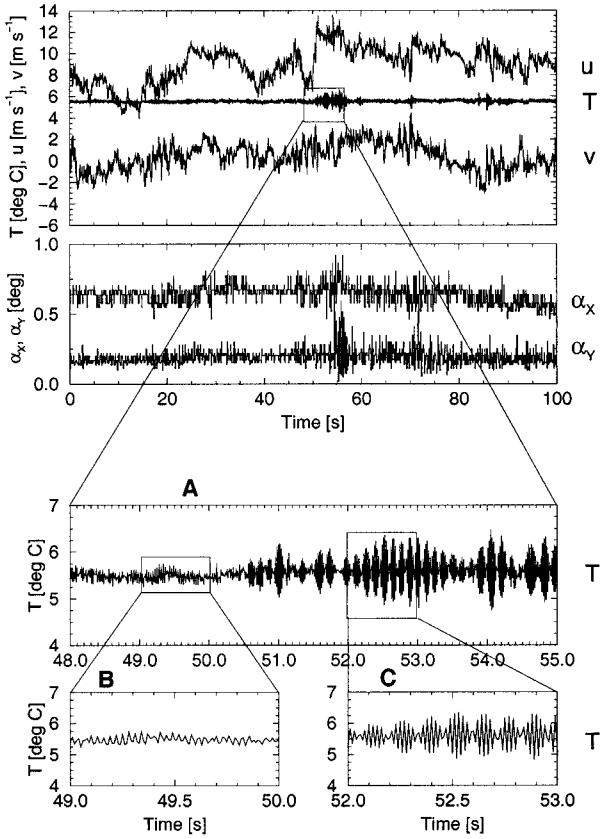

FIG. 11. Time series of temperature T, velocity components u, v and the roll and pitch angles α_X, α_Y measured in the field (run 1) with enlarged portion in details *A*, *B*, and *C*.

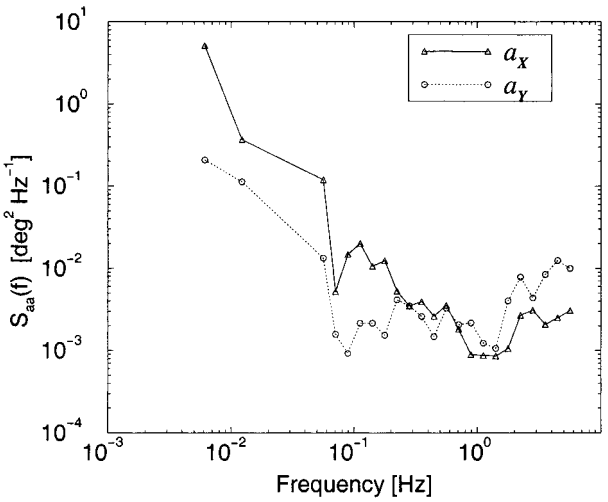

FIG. 12. Variance spectra of the roll α_X and pitch α_Y angles measured in the field (run 1).

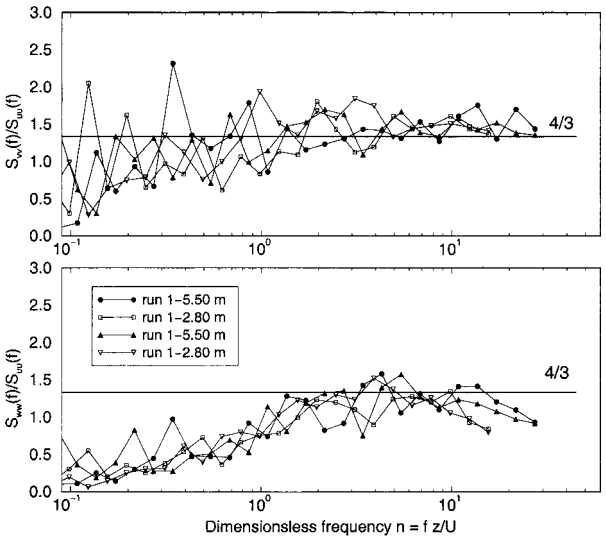

FIG. 13. Ratio (top) $S_{vv}(n)/S_{uu}(n)$ and (bottom) $S_{ww}(n)/S_{uu}(n)$ derived from field data. A 4/3 ratio is plotted for reference, indicating the value predicted by classical theory for isotropic turbulence.

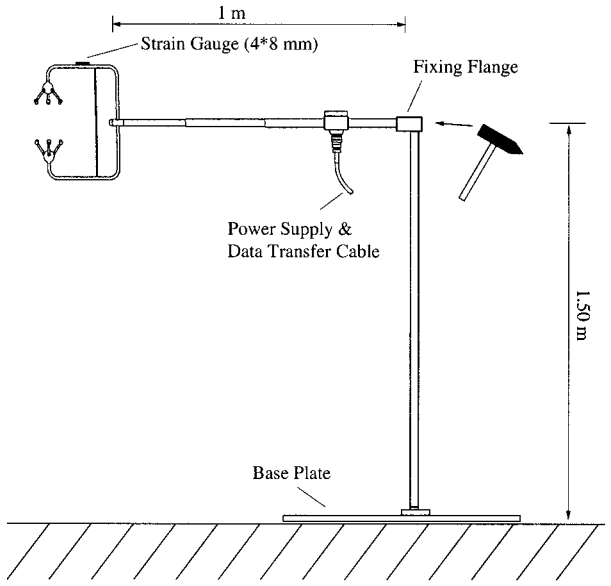

FIG. 14. Experimental setup for laboratory investigations of the tuning-fork effect. The resonances were induced with a light hammer blow.

however, are different from the transfer functions derived by Kaimal et al. (1968) because the geometry of the Solent HS is different from the sonic examined by Kaimal et al. (1968). A quantitative reanalysis following Kaimal et al. (1968) seems straightforward, but it is not part of this work.

c. Tuning-fork effect

To investigate the artifacts in the temperature data observed in the field, further measurements in the laboratory were carried out. The sonic was mounted on a short mast (Fig. 14), much the same way it was attached to the tower in the field. The aluminium mast (a tube, 5 cm in diameter) was fixed on a heavy ground plate (80 kg). At the top of the mast a flange was mounted to fix the sonic in the way recommended by Gill Instruments (1998). A single blow with a light hammer was applied to the mast to induce tuning-fork resonances of the sonic head. The vibrations of the framework were measured with a strain gauge that was fixed at the sonic head. In the first experiment, the amplified signal of the strain gauge was sampled and stored with $f_s = 500$ Hz with a 16-bit analog-to-digital converter. The time series consisted of a 16-s long record. In Fig. 15 smoothed power spectra of the strain-gauge signal from 10 to 250 Hz (the Nyquist frequency f_{Ny}) are presented. At the top of Fig. 15 we show spectra from three time series with induced resonances. For the three lower spectra, the sonic head was fixed to preclude resonance and to investigate the noise of the strain-gauge amplifier. Many significant peaks can be detected in both spectra; most dominant is the peak at 50 Hz that is caused by ambient signals in the laboratory. However, three significant peaks in the upper spectra (designated by arrows) can be clearly seen that are not present in the lower spectra. Peak 1 is at 20 Hz, peak 2 is at about 35 Hz, and peak 3 is at 47 Hz. These three peaks have the same frequency as the artifacts detected in the power spectra of the temperature shown in Fig. 10. Therefore, the presumption of pathlength oscillations caused by tuning-fork resonances of the sonic frame seems to be reasonable. In a second experiment, the strain-gauge signal was sampled with an additional 14-bit analog input of the sonic; this sampling was synchronous with the wind and temperature measurements, and the Nyquist frequency was 50 Hz. From this experiment, the time series of the

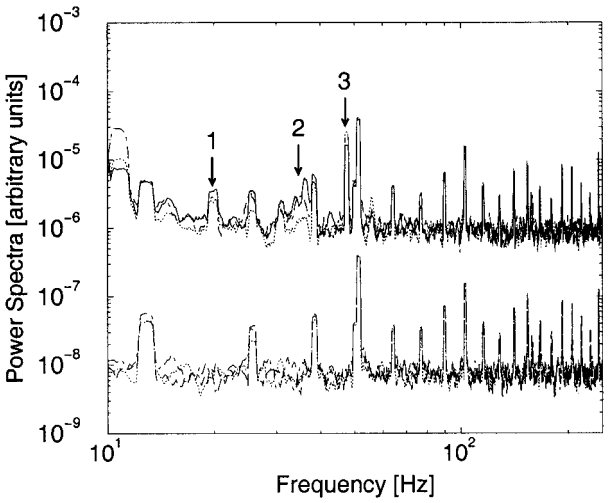

FIG. 15. Power spectra of the strain-gauge signals of three time series (top) with induced vibration of the sonic frame with a light blow by a hammer and (bottom) without vibration.

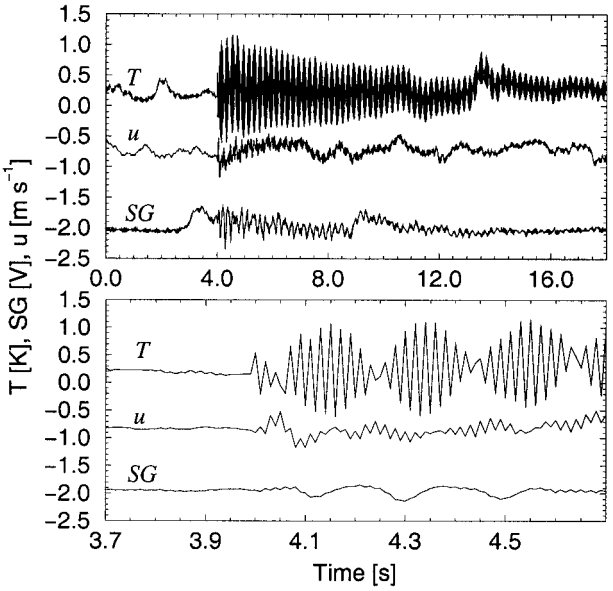

FIG. 16. Time series of the sonic temperature T, strain-gauge signal SG and the velocity component u. The artifacts were induced at t = 4 s by a blow with a hammer.

strain-gauge signal SG, the temperature T, and the velocity component u are shown in Fig. 16. The top part of the figure shows the complete time series of 18 s. The blow occurred at $t = 4$ s; it can be clearly seen in all signals. The maximum amplitude of the temperature oscillation is about 0.9 K, decreasing to a value of $1/e$ of its maximum after about 9 s. In the bottom panel of Fig. 16, a portion of the upper panel is presented with higher time resolution. The temperature time series shown in the lower panel of Fig. 16 has a similar structure as the temperature artifacts that have been observed in the field (see Fig. 11, lower right-hand panel). In the next section, we explain quantitatively why tuning-fork oscillations contaminate the temperature measurements much more drastically than the velocity measurements.

3. Discussion

In order to get more quantitative insight into how the tuning-fork effect contaminates temperature and velocity measurements, let us assume that the pathlength l oscillates with an amplitude a:

$$l(t) = l_0 + a\cos(\omega t), \tag{9}$$

where l_0 is the mean pathlength and ω is the oscillation frequency. Let

$$\tau_1 = \frac{l_1}{c + u} \tag{10}$$

be the travel time of an ultrasonic pulse traveling from the first to the second transducer measured at time t_1, and let

$$\tau_2 = \frac{l_2}{c - u} \tag{11}$$

be the travel time of a second pulse traveling back from the second to the first transducer at a time $t_2 = t_1 + \Delta t$. Here, c is the speed of sound and u is the component of the wind velocity in the direction from the first to the second transducer. We have introduced $l_1 = l(t_1)$ and $l_2 = l(t_2)$. For the sake of simplicity, we assume that the travel times τ_1 and τ_2 are small compared to Δt, and that c and u do not change along the sonic path and during the period between t_1 and t_2. Resolving (10) and (11) for c and u reveals

$$c = \frac{1}{2}\left(\frac{l_1}{\tau_1} + \frac{l_2}{\tau_2}\right) \quad \text{and} \tag{12}$$

$$u = \frac{1}{2}\left(\frac{l_1}{\tau_1} - \frac{l_2}{\tau_2}\right). \tag{13}$$

When measuring c and u with a sonic, it is assumed that the pathlength does not change, that is, the validity of the measurements relies upon the validity of the assumptions $l_1 = l_0$ and $l_2 = l_0$. We arrive at the following equations for the measurement errors $\Delta c = c_m - c$ and $\Delta u = u_m - u$, where c_m and u_m are the measured values and c and u are the true values of sound speed and wind velocity, respectively:

$$\Delta c = \frac{1}{2}\left(\frac{l_0 - l_1}{\tau_1} + \frac{l_0 - l_2}{\tau_2}\right) \quad \text{and} \tag{14}$$

$$\Delta u = \frac{1}{2}\left(\frac{l_0 - l_1}{\tau_1} - \frac{l_0 - l_1}{\tau_2}\right). \tag{15}$$

After some elementary manipulations, we find

$$\Delta c = -\frac{1}{2}\frac{a}{l_0}[(c_m + u_m)\cos(\omega t_1) + (c_m - u_m)\cos(\omega t_2)] \quad \text{and} \tag{16}$$

$$\Delta u = -\frac{1}{2}\frac{a}{l_0}[(c_m + u_m)\cos(\omega t_1) - (c_m - u_m)\cos(\omega t_2)]. \tag{17}$$

Now, we assume that Δt is much smaller than the oscillation period $2\pi/\omega$, and we introduce $t = (t_1 + t_2)/2$. Then we have

$$\cos(\omega t_1) + \cos(\omega t_2) \approx 2\cos(\omega t) \quad \text{and} \tag{18}$$

$$\cos(\omega t_1) - \cos(\omega t_2) \approx -\omega\Delta t\cos(\omega t). \tag{19}$$

This leads to the main results

$$\Delta c = -\frac{1}{2}\frac{a}{l_0}[2c_m\cos(\omega t) - u_m\omega\Delta t\sin(\omega t)] \quad \text{and} \tag{20}$$

$$\Delta u = -\frac{1}{2}\frac{a}{l_0}[2u_m\cos(\omega t) - c_m\omega\Delta t\sin(\omega t)], \tag{21}$$

which we discuss in the remainder of this section.

In (20) the second term is negligible if, as we have assumed, $\omega\Delta t$ is small compared to unity, and if u_m is small compared to c_m, which is practically always fulfilled. That is, we find with very good approximation

$$\Delta c = -\frac{a}{l_0} c_m \cos(\omega t). \tag{22}$$

Since the (virtual) temperature is proportional to the square of the sound velocity, the amplitude of the relative temperature error is $2a/l_0$. That is, we obtain for the amplitude of the temperature artifact caused by the tuning-fork effect

$$\tilde{T} = 2\frac{a}{l_0} T. \tag{23}$$

As an example, we assume $T = 300$ K, $a/l_0 = 1 \times 10^{-3}$ and obtain $\tilde{T} = 0.6$ K, which is comparable to the magnitude of the temperature artifact that we observed. The Solent HS has a pathlength of 15 cm. That is, $a/l_0 = 1 \times 10^{-3}$ implies a pathlength oscillation amplitude of only 0.15 mm.

Now, we discuss the equation for the error that the tuning-fork effect causes in the wind speed measurements, Eq. (21). Here, the relative importance of the first and second terms depend on whether $\omega\Delta t$ is small or large compared to $2u_m/c_m$, which is twice the Mach number: for $\omega\Delta t \ll 2u_m/c_m$, the second term is negligible; for $\omega\Delta t \gg 2u_m/c_m$, however, the first term is negligible. For the Solent HS, the period of the dominating resonance was about 20 ms. The time between two subsequent pulses, Δt, is about 1.1 ms. That is, we find $\omega\Delta t \approx 0.3$, which is one or two orders of magnitude larger than typical Mach numbers in the atmosphere. Therefore, the first term in Eq. (21) is negligible, and we find

$$\Delta u = \frac{1}{2}\frac{a}{l_0} c_m \omega\Delta t \sin(\omega t). \tag{24}$$

As an example, we assume $a/l_0 = 1 \times 10^{-3}$, as before, and assume $c_m = 340$ m s^{-1} and $\omega\Delta t = 0.3$. This leads to a wind velocity artifact amplitude of 5 cm s^{-1}, which is not detectable at moderate or high turbulence intensities.

4. Summary and conclusions

The performance of a new ultrasonic anemometer–thermometer, the Solent-Research HS manufactured by Gill Instruments in Lymington, United Kingdom, was investigated. The sonic's pathlength l is 15 cm and its sampling frequency f_s is 100 Hz. Three wind-velocity components u, v, w and the temperature T were measured in the laboratory under quiet conditions and in the field at wind speeds of about 10 m s^{-1}. The power spectra of u, v, w, and T measured in the laboratory follow a $-5/3$ power law at moderate frequencies. At frequencies higher than $\overline{u}/l$ (here $\overline{u}$ is the mean wind speed along a given path), there is a roll-off in all spectra, an effect caused by the spatial averaging along the finite pathlength. Over the bandwidth of $f_s/2 = 50$ Hz, the standard deviations due to uncorrelated noise amount to 0.02 m s^{-1} for u, v, and w and to 0.02 K for T. In the field, the spectra of u, v, and w show a clean $-5/3$ power law in the inertial subrange, except for a flattening at frequencies larger than 30 Hz, which is probably an artifact caused by aliasing. In the inertial subrange, the ratio of the spectra of the transverse and longitudinal velocity components was close to 4/3, the ratio predicted for isotropic turbulence by the classical theory. The temperature spectra measured in the field were severely contaminated at frequencies larger than about 5 Hz. Closer inspection of the T time series revealed an amplitude-modulated artifact (see also the appendix). Since no similar artifact was apparent in the velocity spectra, the artifacts were presumed to result from oscillations of the sonic's pathlengths induced by oscillations of the tower, which was exposed to a turbulently changing wind field. We reproduced these artifacts in the laboratory by controlled blows on the sonic's attachment. The mechanical oscillations, which we refer to as tuning-fork resonances, were measured with a strain gauge attached to the sonic, and they correlated well with the artifacts in T recorded simultaneously. The dominating artifact was found at 47 Hz, which is close to the sonic's Nyquist frequency, $f_s/2 = 50$ Hz. Temperatures measured with a sonic are very sensitive to small changes in the pathlength. For example, pathlength changes must be kept below 0.02 mm in order to keep the amplitude of the resulting temperature artifact below 0.02 K, which is the standard deviation of the investigated sonic. We have demonstrated that the tuning-fork effect can easily cause temperature artifacts that far exceed the system noise. We recommend appropriate changes in the mechanical design of the Solent-Research HS so that the full potential of the system will be available under difficult conditions in the field.

Acknowledgments. We thank Ulrich Teichmann and Thomas Conrath for their assistance in performing the field experiments. Thanks are also due to John Gaynor and an anonymous reviewer for their valuable comments on the manuscript, and to Chris Fairall and Mikhail Charnotskii for helpful suggestions on an earlier version of the paper.

APPENDIX

"Tuning-Fork Effect"

Consider a monochromatic temperature artifact caused by mechanical tuning-fork resonance of the sonic:

$$T(t) = \hat{T} \exp(i\omega_r t + \varphi_a). \tag{A1}$$

When this temperature signal is sampled at a frequency ω_s, the sampling time series is

$$T_j = T(t_j) = T\left(j\frac{2\pi}{\omega_s}\right) \tag{A2}$$

$$= \hat{T}\exp\left[i\left(j\pi\frac{\omega_r}{\omega_{\mathrm{Ny}}} + \varphi_a\right)\right], \tag{A3}$$

where

$$\omega_{\mathrm{Ny}} = \frac{\omega_s}{2} \tag{A4}$$

is the Nyquist frequency. We express ω_r in terms of ω_{Ny},

$$\omega_r = n\omega_{\mathrm{Ny}} + \Delta\omega, \tag{A5}$$

where n is the largest possible integer number, such that $\Delta\omega/\omega_{\mathrm{Ny}}$ is smaller than 1 but not smaller than zero. We obtain

$$T_j = \hat{T}\exp\left[i\left(j\pi n + j\pi\frac{\Delta\omega}{\omega_{\mathrm{Ny}}} + \varphi_a\right)\right] \tag{A6}$$

$$= \hat{T}\exp(ij\pi n)\exp\left(ij\pi\frac{\Delta\omega}{\omega_{\mathrm{Ny}}}\right)\exp(i\varphi_a). \tag{A7}$$

If n is even, then the factor $\exp(ij\pi n)$ is 1 for each integer j. If n is odd, however, then $\exp(ij\pi n)$ causes an oscillation between $+1$ and -1 at the Nyquist frequency; that is, then $\exp(ij\pi n)$ is $+1$ for even j and -1 for odd j.

In the case of an odd n, the factor $\exp[ij\pi(\Delta\omega/\omega_{\mathrm{Ny}})]$ modulates the amplitude of the Nyquist frequency oscillation. The modulation factor can be rewritten,

$$\exp\left(ij\pi\frac{\Delta\omega}{\omega_{\mathrm{Ny}}}\right) = \exp\left(i\frac{t_j}{\frac{\pi}{\omega_{\mathrm{Ny}}}}\pi\frac{\Delta\omega}{\omega_{\mathrm{Ny}}}\right) = \exp(i\Delta\omega t_j), \tag{A8}$$

and we obtain the amplitude modulation frequency:

$$\omega_m = \Delta\omega. \tag{A9}$$

The artifact observed in the data of this study indicates an odd n (probably $n = 1$) and a modulation frequency $f_m = \Delta\omega/(2\pi)$ of about 8 Hz.

REFERENCES

Gill Instruments Ltd., 1998: Horizontally symmetrical research ultrasonic anemometer. Tech. Rep. Doc. 1199-PS-0003-Iss5, 43 pp. [Available from Gill Instruments Ltd., Saltmarsh Park, 67 Gosport Street, Lymington, Hampshire, SO41 9EG, United Kingdom.]

Grelle, A., and A. Lindroth, 1994: Flow distortion by a Solent sonic anemometer: Wind tunnel calibration and its assessment for flux measurements over forest and field. *J. Atmos. Oceanic Technol.,* **11,** 1529–1542.

Haugen, D. A., and J. C. Kaimal, 1975: A comparison of balloon-borne and tower-mounted instrumentation for probing the atmospheric boundary layer. *J. Appl. Meteor.,* **14,** 540–545.

Henjes, K., P. K. Taylor, and M. J. Yelland, 1999: Effect of pulse averaging on sonic anemometer spectra. *J. Atmos. Oceanic Technol.,* **16,** 181–184.

Horst, T. W., 1973: Spectral transfer functions for a three-component sonic anemometer. *J. Appl. Meteor.,* **12,** 1072–1075.

Kaimal, J. C., and J. E. Gaynor, 1991: Another look at sonic thermometry. *Bound.-Layer Meteor.,* **56,** 401–410.

——, J. C. Wyngaard, and D. A. Haugen, 1968: Deriving power spectra from a three-component sonic anemometer. *J. Appl. Meteor.,* **7,** 827–837.

——, ——, Y. Izumi, and O. R. Cote, 1972: Spectral characteristics of surface-layer turbulence. *Quart. J. Roy. Meteor. Soc.,* **98,** 563–589.

Mitsuta, Y., 1966: Sonic anemometer–thermometer for general use. *J. Meteor. Soc. Japan,* **44,** 12–24.

Muschinski, A., and R. Roth, 1993: A local interpretation of Heisenberg's transfer theory. *Contrib. Atmos. Phys.,* **66,** 335–346.

Siebert, H., and U. Teichmann, 2000: The behavior of an ultrasonic under cloudy conditions. *Bound.-Layer Meteor.,* **94,** 165–169.

Wilczak, J. M., S. P. Oncley, and S. A. Stage, 2000: Sonic anemometer tilt correction algorithm. Preprints, 14*th Symp. on Boundary Layers and Turbulence,* Aspen, CO, Amer. Meteor. Soc., 153–156.

Wyngaard, J. C., and S.-F. Zhang, 1985: Transducer-shadow effects on turbulence spectra measured by sonic anemometers. *J. Atmos. Oceanic Technol.,* **2,** 548–558.